Hindawi
Geofluids
Volume 2023, Article ID 5884572, 10 pages
https://doi.org/10.1155/2023/5884572

Review Article

Using a Synthetic Borehole Model to Determine the Pore Aspect Ratio Dependence of Velocities from Acoustic Well-Logging Data

Xiao Feng,[1] Tianyang Li,[2] Bingrui Du,[3] and Wenxin Kong[2]

[1]*School of Economics and Business Administration, Chongqing University, Chongqing 400044, China*
[2]*School of Resources and Safety Engineering, Chongqing University, Chongqing 400044, China*
[3]*Institute of Geophysical and Geochemical Exploration, Chinese Academy of Geological Sciences, Langfang 065000, China*

Correspondence should be addressed to Tianyang Li; tli@cqu.edu.cn and Bingrui Du; 125110371@qq.com

Received 15 August 2022; Accepted 23 September 2022; Published 20 March 2023

Academic Editor: Zhongwei Wu

Revealing the elastic wave properties of carbonate rocks with complex pore structures and improving the reliability of carbonate reservoir descriptions have always been a global challenge in the field of carbonate geophysical exploration. In this study, we established a synthetic borehole model by selecting different particle sizes of cement, carbonate cuttings, and micro-silicon as the matrix, and silicon disks as the pores in carbonate rocks. We conducted four sets of low-porosity (0-3%) borehole models with different pore aspect ratios (ARs) and measured the P- and S-wave velocities (V_P and V_S) at the well-logging scale obtained from an acoustic logging system with one source and two receivers. The results indicate that the relationship between velocities and porosities in these borehole models follows a linear relation, with the pore AR significantly influencing the velocities at any given porosity. The velocity variation caused by pore AR reaches 560 m/s and 410 m/s at 3% porosity for the P-wave and S-wave within the AR range of 0.017-0.13. The theoretical DEM models provide a high and broad estimation of V_P and V_S at the well-logging scale in our measurement. They could perform better in fractured formation than in dissolved porous formation in carbonate reservoirs. The linear relation of V_P and V_S is independent of the pore AR and is effective for both fractured and dissolved porous formations. The change of V_P/V_S in different pore AR is more responsive to porosity and nonlinear dependent on the pore AR. The relationship between the defined normalized V_P and V_S indicates the pore AR has a more significant effect on V_S than V_P in our model. The constructed borehole models provide a unique opportunity for evaluating the availability of rock physics models at an acoustic logging scale. The study's findings have significant implications for improving the reliability of carbonate reservoir descriptions and enhancing the accuracy of geophysical exploration in carbonate rocks with complex pore structures.

1. Introduction

Accurate characterization of pore structure in unconventional oil and gas systems has proven to be challenging due to their complex morphology and the strong diagenesis and tectonism [1–3]. Currently, techniques such as acoustic emission experiments, acoustic logging, and seismic monitoring, which are based on elastic wave theory, have become important methods for detecting underground structures, oil and gas minerals, and geothermal resources. However, the changes in pore structure can significantly impact the elastic frame moduli of naturally occurring rocks, resulting in changes in their elastic wave velocities [4–9].

The pore aspect ratio (AR; the ratio of the minor axis to the major axis) dependence of velocities of crustal rocks, affecting the energy exchange between the formation and pore fluids, has been widely reported [5, 10–13]. The power relationship between elastic wave velocities and pore AR has been proposed in the theoretical model (e.g., [14, 15]) and rock physics experiments at the core scale (e.g., [4, 8]). However, the frequency dependence of velocities can lead to errors and difficulties in the dynamic elastic parameters of rocks when attempting to apply the laboratory results in the ultrasonic frequency band (0.1 MHz-10 MHz) to the acoustic well-logging interpretation in the medium-frequency range (20 Hz-200 kHz) [16–19] and seismic

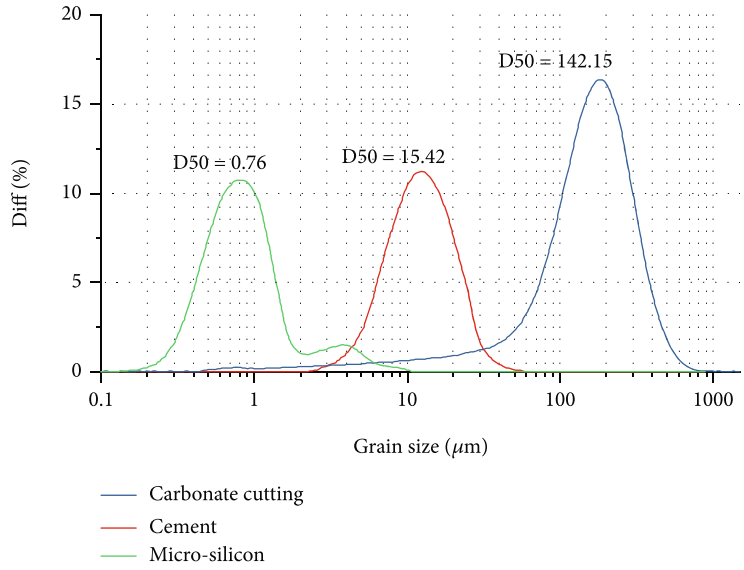

Figure 1: Particle size distribution of the three solid-phase materials.

exploration (~100 Hz) [20]. It has always been a research hotspot in the field of geophysics to establish the relationship between the elastic wave properties of rocks across frequency bands. Additionally, considering the complex well-logging environment, it is challenging and inaccurate to obtain detailed information about the pore structure beyond porosity using conventional well-logging data [21].

Developing rock physics models with controlled pore structures is an urgent need to quantitatively investigate the effects of pore structures on wave velocity and attenuation (e.g., [4, 22–25]). The artificial sandstone cores are relatively mature and simple after decades of development. Usually, quartz sand with different grain sizes and cementing agents (such as Plexiglas and epoxy resin) are mixed to simulate the sandstone. Aluminum, copper, and tin foil are the common materials used to simulate the fractures, interparticle pores, and vugs in the formation [4, 26, 27]. However, for carbonate rocks, the existing methods (e.g., sheet combination method, cutting simulation method, interpolation method, and dissolution method) are more applicable for small-scale artificial cores for the following reasons: (1) the epoxy resin is too expensive to be widely used in well-logging scale models. (2) The consistency after adding epoxy resin is too high to ensure uniform mixing. (3) The final properties of rock physics models are influenced by the times and pressures in the compaction process, while it is difficult to control these parameters in the large-scale models. (4) ccurately controlling pore parameters and distribution in the large-scale models remains difficult with existing methods [28, 29].

To simulate the acoustic well logging in the carbonate reservoir in the laboratory, we have developed a new borehole model with controlled pore structures and examined the influences of pore characteristics on the elastic properties via a homemade acoustic logging system [12]. In this study, we further focus on the pore AR dependence of velocities on a larger set of borehole models, including one blank model without pores and 20 models with different pore ARs and porosities. This work aims to provide a new dataset of measured P- and S-wave velocities (V_P and V_S) at the well-logging scale, which can serve as a preliminary reference for acoustic well-logging interpretation in the carbonate reservoir.

2. Methods

2.1. Borehole Model Building. Cement has been widely used in rock mechanics experiments for a long time [30, 31]. Both theoretical and experimental studies have shown that particle gradation determines the cement properties (e.g., density and strength) under the same mass ratio of cement and other matrix materials [32]. To consolidate the model matrix tightly and closely mimic the properties of the target formation, we choose cement slurry, carbonate cuttings, and microsilicon powder with different grain sizes as the solid phases for the borehole model. The carbonate cuttings are clean crystalline grains with a grain size of 150 μm, and the pure calcite content is over 98%. The microsilicon with 1 μm particle size is used to effectively prevent the sedimentation during the curing process. The microsilicon powder has a pure SiO_2 content of over 97%.

The particle size distribution of the above three solid-phase materials are measured by the Bettersize2000 laser particle size distribution instrument (Figure 1). The average particle sizes of carbonate cuttings, cement, and microsilicon powder are 142.15 μm, 15.42 μm, and 0.76 μm, respectively. However, the addition of carbonate cuttings and microsilicon powder makes the cement slurry system less fluid and challenging to mix uniformly. The effect of different ratios of cement slurry and carbonate cuttings on the matrix fluidity is shown in Table 1. After considering the matrix density and fluidity of the cement slurry, the mass ratio of carbonate cuttings, cement, and water is determined as 1 : 1 : 0.4. The mass radio of microsilicon is 1% of the matrix material. In

Table 1: The fluidity of the matrix with different ratios of cement slurry and carbonate cuttings.

Sets	Cement/kg	Water/kg	Carbonate cuttings/kg	Ratio	Fluidity
1	50	20	75	1 : 1.5 : 0.4	No fluidity
2	50	20	62.5	1 : 1.25 : 0.4	Low-medium fluidity
3	50	20	50	1 : 1 : 0.4	Medium fluidity
4	50	20	37.5	1 : 0.75 : 0.4	Medium-high fluidity
5	50	20	25	1 : 0.5 : 0.4	High fluidity

addition, graft polymers of sulfonated aldehyde-ketone condensation as the drag reducer and polymers of polyether and organic silicon as the defoamer are added to the matrix to discharge the bubbles formed during agitation. Finally, the required amount of materials for each model is list in Table 2.

In this study, "penny-shaped" silicone disks with different thicknesses and diameters, whose properties are comparable to fluids with relatively low density and propagation velocity, are distributed in the borehole model to simulate the different pore structures in carbonate rocks. A vertical hole with 76 mm width and 600 mm depth was drilled in the center of the model and filled with water to simulate the petroleum drilling procedure. Figure 2 shows the construction process of the borehole model.

The cores were left to cure for 28 days at room temperature (Figure 3(a)) and then examined under a metallurgical microscope (Figures 3(b) and 3(c)). The shiny areas are the carbonate cutting, the dark areas are the cement hydration products, and the black areas are the primary pores resulting from the undischarged bubbles. The porosity and permeability were obtained from the gas measurement. The primary porosity is 24.36%, the permeability is low (<0.029 mD), and the density is 2.12 g/cm^3. The density difference is less than 0.05 g/cm^3, indicating that the matrix properties are more similar to the actual carbonate rocks than those of the simple cement system. Finally, we constructed four sets of low-porosity (0.6-3%) borehole models with varying pore AR of 0.017, 0.033, 0.067, and 0.13 (Table 3).

2.2. Velocity Measurements. To simulate the acoustic well-logging in the laboratory, we cooperated with Yangzhou Oriental Ultrasound Technology Co. Ltd. to design an acoustic logging system with one ring-emitting piezoelectric source and two piezoelectric receivers (as shown in Figure 4). The dominant frequency of the piezoelectric source is 20-40 kHz. This equipment is placed in the central borehole filled with water. The source-receiver distances are 22.2 cm and 36.5 cm for the two receivers. The typical waveforms received by the receivers are shown in Figure 5. The velocities in the borehole model are calculated from the differential arrival times of the P- and S-waves between the two receivers:

$$V_i = \frac{\Delta l}{t_{2i} - t_{1i}}, \quad (1)$$

where V_i is the velocity of ith phases (P-, S-, and Stoneley waves) in km/s, Δl is the length between the two receivers in mm, while t_{1i} and t_{2i} are the picked ith arrival times of all phases waves of the two received signals in μs. The main source of errors in the velocity measurement is associated with the picking of travel times from the acquired raw waveforms.

Table 2: The total amount of matrix materials for each borehole model.

Materials	Mass/kg	Grain size/μm
Carbonate cuttings	50	142.15
Cement	50	15.42
Water	20	Fluid
Microsilicon	1	0.76
Drag reducer	0.2	Fluid
Defoamer	1	Fluid

3. Results

Porosity is the key parameter for characterizing materials microstructures and is the main output from well-log interpretation [33]. A broadly accepted consensus is that the complex pore structures cause the wide scatter in the velocity-porosity relationship for the carbonate rocks [4, 8, 13]. The measurements from our models show that both the V_P and V_S decrease with the increase in porosity at the same pore AR (Figure 6). The relationship can be well-described by a simple negative linear function, which is similar to the results from rock physics experiments [34, 35].

In addition, pore AR has a remarkable effect on elastic wave propagation [36–38], affecting the energy exchange between the formation and pore fluids. However, recent researches only focus on building quantitative trends between the velocity and pore type at the core scale [8]. We built four sets of borehole models with different pore AR of 0.017, 0.033, 0.067, and 0.13. The velocity variation caused by pore AR is as high as 560 m/s and 410 m/s at 3% porosity for the P-wave and S-wave within the AR range of 0.017-0.13 in our experiments. It should be noted that more silicon disks are required to achieve the same porosity when pore AR is low in each model set.

The ratio of microstructure size (d) to wavelength (λ) affects velocity in the porous media. In the past decades, several studies have tested effective medium theories (EMT) in the long-wavelength limit situation ($\lambda > d$), seeking to relate the rock minerals and pore structures to the effective elastic

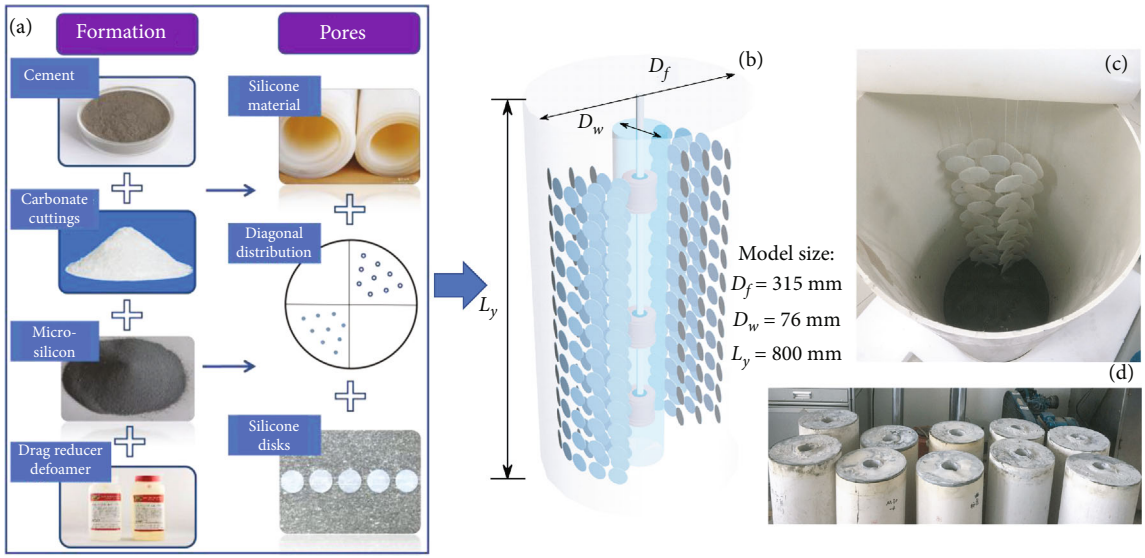

Figure 2: (a) The material and building process of the borehole model. (b) A schematic physical model with the homemade acoustic logging system. (c) The distribution of the silicone disks. (d) The borehole models after coring in the center.

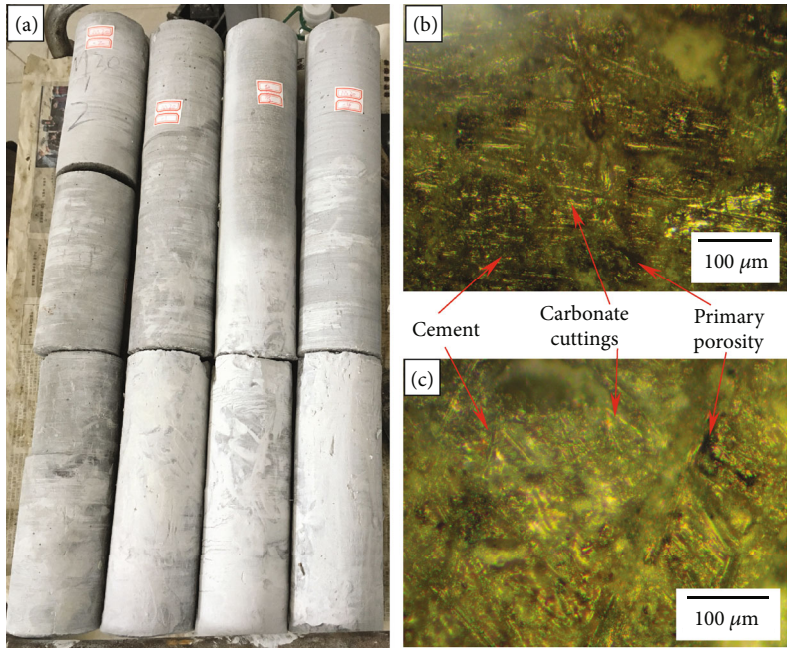

Porosity (%)	Permeability (mD)	Slip coefficient	Density (g/cm³)	Compressive strength (MPa)
12.36	0.029	0.354	2.12	45

Figure 3: The physical property (porosity, permeability, slip coefficient, density, and compressive strength) of the cores from the borehole models. (a) The diameter and length of the extracted cores are 76 mm and 600 mm. (b, c) The metallurgical map of the matrix.

properties on a macroscopic scale by assuming different pore ARs [35, 39–41]. In this study, the dominant frequency of the acoustic logging system is 20-40 kHz, and the wavelength is 50-100 mm. The size of the silicon disks is 30 mm; thus, our model is within the scope of the long-wavelength range. Therefore, we analyze the pore AR dependence of velocities in the following sections and compare it with those of EMT models to gain further insight into the phenomena that control elastic wave propagation in the borehole models. The previous study has indicated that the differential effective medium (DEM) model [42] shows closer outcomes to our results in the borehole models [12]. Therefore, we use the DEM model to calculate the theoretical velocities of the borehole model with different pore ARs. The values of the

Table 3: Model sets and the corresponding parameters.

Sets	Models	φ (%)	h (mm)	d (mm)	AR	N
A	A#0.6	0.6	0.5	30	0.017	12 × 24
	A#1.2	1.2				12 × 48
	A#1.8	1.8				24 × 36
	A#2.4	2.4				24 × 48
	A#3.0	3				24 × 60
B	B#0.6	0.6	1		0.033	6 × 24
	B#1.2	1.2				12 × 24
	B#1.8	1.8				12 × 36
	B#2.4	2.4				12 × 48
	B#3.0	3				12 × 60
C	C#0.6	0.6	2		0.067	6 × 12
	C#1.2	1.2				12 × 12
	C#1.8	1.8				12 × 18
	C#2.4	2.4				12 × 24
	C#3.0	3				12 × 30
D	D#0.6	0.6	4		0.13	6 × 6
	D#1.2	1.2				6 × 12
	D#1.8	1.8				6 × 18
	D#2.4	2.4				6 × 24
	D#3.0	3				6 × 30

Note: φ is the porosity of the borehole model; d and h are the diameter and thickness of the silicon disks, respectively; N is the total number of silicon disks in each model.

input parameters in the DEM model are summarized in Table 4. Other parameters used in these theoretical models are the same as those of the borehole model. The results show that the theoretical DEM models provide a high estimation of the V_P and V_S, and the deviations become larger as pore AR increases. It is worth mentioning that relatively small variations of wave velocities are observed at the well-logging scale. Therefore, the theoretical model is more suitable for fractured formation than the dissolved porous formation in carbonate reservoirs.

4. Discussion

4.1. $V_P - V_S$ Linear Relation. The relation between the V_P and V_S for sandstone is usually constant. Our newly developed carbonate borehole models follow a linear $V_P - V_S$ relation (Figure 7), which has been verified from the test of carbonate samples [43]. The high determinant coefficient (R^2 value) indicates that the linear relation of V_P and V_S is independent of the pore AR.

Wang et al. [24] introduced a general velocity model for carbonate rocks determined by core measurements:

$$\begin{cases} V_P = V_{P0} - a_1\varphi_p - a_2\dfrac{\varphi_s}{\mathrm{AR}^{c_1\varphi_s+c_2}}, \\ V_S = V_{S0} - b_1\varphi_p - b_2\dfrac{\varphi_s}{\mathrm{AR}^{d_1\varphi_s+d_2}}, \end{cases} \quad (2)$$

where a_1, a_2, b_1, b_2, c_1, c_2, d_1, and d_2 are empirical parameters; φ_p represents the primary porosity; φ_s represents the secondary porosity; V_{P0} and V_{S0} represent the P- and S-wave velocities of the solid matrix, respectively.

Then, Equation (1) can be further rewritten as follows:

$$V_S = V_{S0} - b_1\varphi_p - \frac{b_2\varphi_s}{\left(a_2\varphi_s/V_{P0} - a_1\varphi_p - V_P\right)^{g(\varphi_s)}}, \quad (3)$$

$$g(\varphi_s) = \frac{d_1\varphi_s + d_2}{c_1\varphi_s + c_2}. \quad (4)$$

Based on the measured data, the fitting parameters c_1 and d_1 range from -1 to 0; c_2 and d_2 range from 0.5 to 1. In our study, the secondary porosity is low (<3%). Therefore, the $g(\varphi_s)$, related to the secondary porosity, is close to 1. Then, Equation (2) could be simplified as follows:

$$V_S = V_{S0} - \frac{b_2}{a_2}V_{P0} + \left(\frac{a_1b_2}{a_2} - b_1\right)\varphi_p + \frac{b_2}{a_2}V_P. \quad (5)$$

The V_{P0}, V_{S0}, and φ_p are related to the solid matrix and constant in the same model. In addition, the fitting parameters in Equation (4) (i.e., a_1, a_2, b_1, and b_2) are only related to porosity and independent of the pore AR, which means that

Figure 4: The homemade acoustic logging system with one source and two receivers.

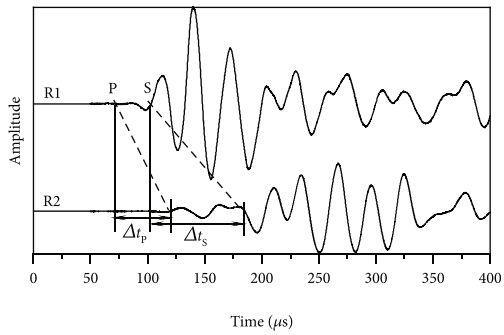

Figure 5: The received waveforms from one borehole model. The differential arrival times of P- and S-waves between the two receivers (R1 and R2 in Figure 4) are used to calculate the wave velocities.

the linear relation between V_P and V_S is effective for different pore AR conditions. Combined with the results of the same linear relation between V_P and V_S in our borehole models, the method for V_S prediction from well-logging data can be used for carbonate formations with fractures, intraparticle pores, or vugs.

4.2. $V_P - V_S$ Ratio. Seismic tomographic results have revealed the importance of V_P/V_S as a diagnostic of the physical cause of a seismic anomaly [44, 45]. Although geophysicists have widely recognized the importance of liquid compressibility in changing V_P/V_S [46], the effect of pore geometry on V_P/V_S has not been commonly acknowledged. In sandstones, the pore structure is simple and V_P/V_S is relatively stable. According to classical elastic theory, V_P/V_S is approximately equal to 1.732 when the Poisson's ratio is 0.25. However, caution is needed when applying the

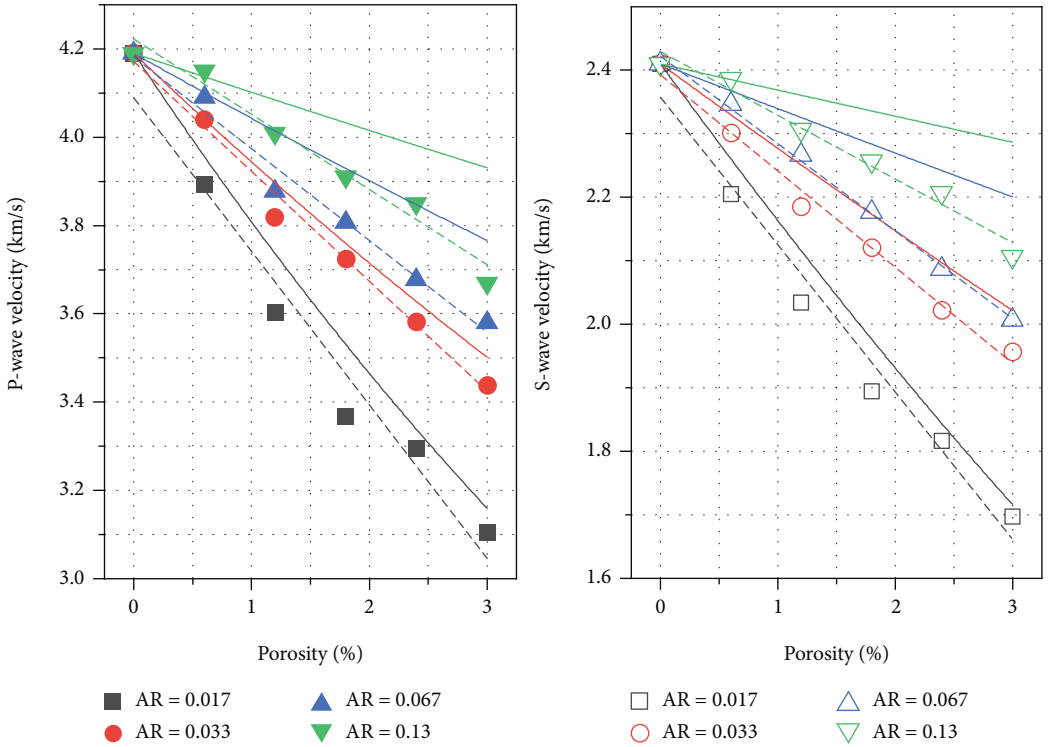

Function	$V_p = a + b \times \varphi$				$V_s = a + b \times \varphi$			
AR	0.017	0.033	0.067	0.013	0.017	0.033	0.067	0.130
a	4.088	4.172	4.182	4.222	2.357	2.392	2.422	2.430
b	−0.347	−0.249	−0.208	−0.171	−0.232	−0.151	−0.137	−0.101
R^2	0.951	0.987	0.978	0.965	0.969	0.988	0.996	0.970

(a) (b)

Figure 6: The V_P (solid points) and V_S (hollow points) of the four model sets. The dashed lines are fitted by linear functions for the different porosities. The solid lines are obtained using DEM concepts with pore AR of 0.017, 0.033, 0.067, and 0.13.

Table 4: Parameters used for DEM model calculation.

Materials	Density (g/cm^3)	V_P (m/s)	V_S (m/s)
Matrix	2.41	4190	2410
Silicon disk	1.24	1326	848

suitability of this relation in carbonate rocks due to the variability of pore structures. To quantitatively describe the V_P/V_S variation with pore AR, we calculate the change in V_P/V_S as

$$\Delta\left(\frac{V_P}{V_S}\right) = \frac{V_P}{V_S}\bigg|_{\text{AR=high}} - \frac{V_P}{V_S}\bigg|_{\text{AR=low}}. \quad (6)$$

As shown in Figure 8, the $\Delta(V_P/V_S)$ is always lower than 0 and has a positive response to porosity, while the influence of pore AR appears to be nonlinear. Due to the low number of models, the accurate relation between pore AR and the $\Delta(V_P/V_S)$ cannot be proposed in this study. Therefore, we observe the same negative $\Delta(V_P/V_S)$ trend from the DEM modelling. The maximum change in V_P/V_S appears at model set C (i.e., AR = 0.067). Overall, the $\Delta(V_P/V_S)$ is more responsive to porosity and nonlinear dependent on the pore AR, which indicates a complex effect of pore AR on V_P/V_S in carbonate rocks.

4.3. Normalized Velocity. The pore AR influences V_P and V_S differently based on the above analysis. Therefore, we compare the velocities within the same pore AR window. The lower and upper pore AR bounds for the velocities analysis are 0.017 and 0.13, and the normalized velocities (V_{pn} and V_{sn}), which quantitatively represent the pore AR dependence of velocities, are defined as

$$\begin{cases} V_{pn} = \dfrac{V_P|_{\text{AR=0.13}}}{V_P|_{\text{AR=0.017}}}, \\ V_{sn} = \dfrac{V_S|_{\text{AR=0.13}}}{V_S|_{\text{AR=0.017}}}. \end{cases} \quad (7)$$

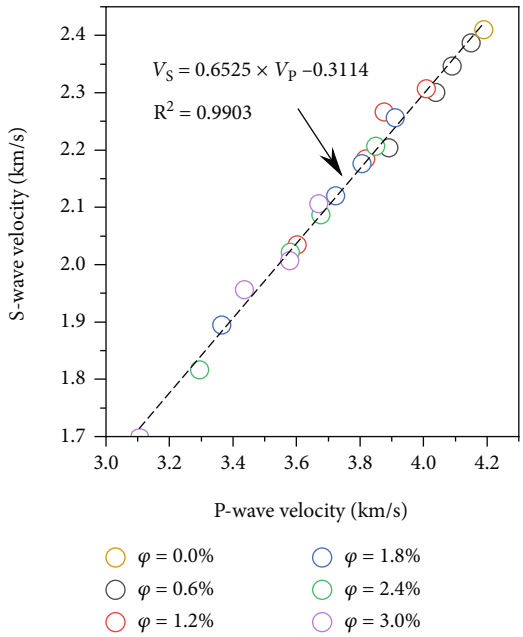

Figure 7: The linear relations of V_P and V_S measured from the four model sets.

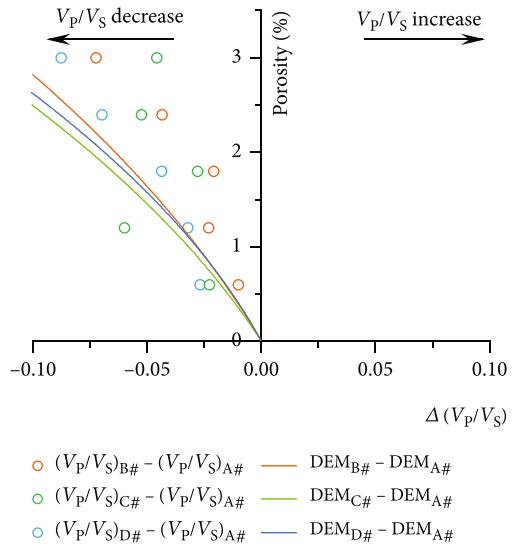

Figure 8: The variation in V_P/V_S with different pore ARs.

The V_P and V_S usually increase with pore AR and follow a power law; thus, the V_{pn} and V_{sn} are higher than 1 (Figure 9). The V_{pn} and V_{sn} both increase by the porosity. The relationship between V_{pn} and V_{sn} follows a linear function where the R^2 value is as high as 0.97. V_{sn} is always higher than V_{pn} with a slope of 1.326, which means the pore AR has a greater effect on V_S than V_P in our model. Interestingly, the calculation from the DEM model shows an astonishing similarity with the trends from our results. Overall, the results suggest that the observed $V_{pn} - \varphi$ and $V_{sn} - \varphi$ relationship for carbonate rocks is influenced by the pore structure.

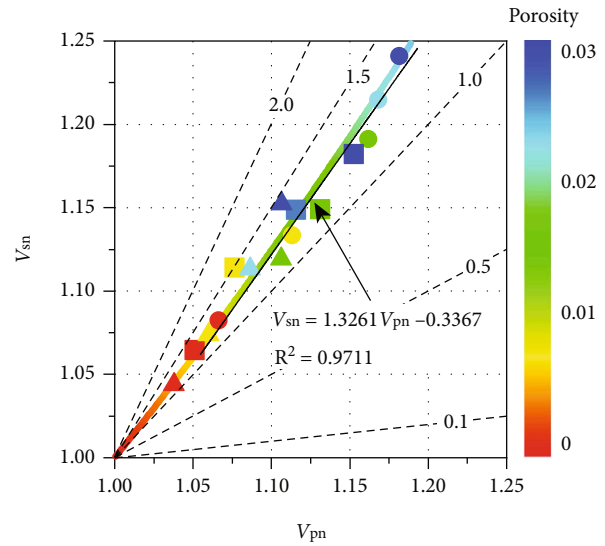

Figure 9: The normalized V_P and V_S in different porosity models. The dashed lines indicate the slopes. The coloured line is the prediction based on the DEM modelling.

Like any artificial core experiment, the results obtained from our on ideal borehole models have their share of pitfalls in view of the isolated "penny-shaped" pores. First, the P-wave velocity and density of silicon disks are similar to those of water, while the V_S of this material is in low comparability to fluid typically encountered in crustal materials. Second, our borehole model ignores the interaction between the solid matrix and the pores/pore fluids, which is also crucial for their elastic wave velocities [47, 48]. However, in this study, we only focus on the effect of pore structures on velocities. The synthetic borehole models are simplified but similar to the actual case, and the elasticity contrasts between the matrix and pore fluids. Nevertheless, our borehole model is suitable for various petrophysical experiments such as acoustic wave characteristics, electrical characteristics, and seepage mechanisms. The results from our borehole model could be a stepping stone for understanding the velocity variation at lower frequencies compared to the conventional rock physics model.

5. Conclusions

By choosing different particle sizes of cement, carbonate cuttings, and microsilicon as the matrix and silicon disks with different AR as the pores in carbonate rocks, we built four sets of low-porosity borehole models and provided a new dataset of the V_P and V_S at lower frequencies obtained from an acoustic logging system with one source and two receivers. This study focuses on the pore AR dependence of velocities and reaches the following key conclusions:

(1) The relation between velocities and porosities measured at the well-logging scale follows a linear function. Meanwhile, the velocity variation caused by pore AR can reach 560 m/s and 410 m/s at 3%

porosity for the P-wave and S-wave within the AR range of 0.017-0.13 in our experiments

(2) The theoretical DEM models overestimate the V_P and V_S. The deviations between the theoretical velocities at the rock physics scale and the measured results at the well-logging scale gradually increase with AR increase, especially when AR is over 0.05, indicating better performance in fractured formations than dissolved porous formations in carbonate reservoirs

(3) The high determinant coefficients indicate that the linear relation of V_P and V_S is independent of pore AR and is effective for both fractured or dissolved porous formation. The change of V_P/V_S in different pore AR is more responsive to porosity and nonlinear dependent on the pore AR. The relationship between the defined normalized V_P and V_S indicates that the pore AR has a greater effect on V_S than V_P

Conflicts of Interest

The authors declare that they have no conflicts of interests.

Acknowledgments

This work was jointly funded by the National Natural Science Foundation of China (Grant nos. 42204058 and 42104071), the Science Foundation of Chongqing (Grant no. CSTB2022NSCQ-MSX1660), and the National Nonprofit Institute Research Grant of IGGE (Grant no. AS2022J03).

References

[1] E. Flügel, *Microfacies of Carbonate Rocks: Analysis, Interpretation and Application*, Springer Science & Business Media, 2004.

[2] H. Mehrabi, M. Mansouri, H. Rahimpour-Bonab, V. Tavakoli, and M. Hassanzadeh, "Chemical compaction features as potential barriers in the Permian-Triassic reservoirs of southern Iran," *Journal of Petroleum Science and Engineering*, vol. 145, pp. 95–113, 2016.

[3] H. Rahimpour-Bonab, H. Mehrabi, A. H. Enayati-Bidgoli, and M. Omidvar, "Coupled imprints of tropical climate and recurring emergence on reservoir evolution of a mid Cretaceous carbonate ramp, Zagros Basin, Southwest Iran," *Cretaceous Research*, vol. 37, pp. 15–34, 2012.

[4] T. Li, R. Wang, Z. Wang, and Y. Wang, "Experimental study on the effects of fractures on elastic wave propagation in synthetic layered rocks," *Geophysics*, vol. 81, no. 4, pp. D441–D451, 2016.

[5] T. Li, Z. Wang, N. Yu, R. Wang, and Y. Wang, "Numerical study of pore structure effects on acoustic logging data in the borehole environment," *Fractals*, vol. 28, article 2050049, 2020.

[6] G. Njiekak, D. R. Schmitt, and R. S. Kofman, "Pore systems in carbonate formations, Weyburn field, Saskatchewan, Canada: micro-tomography, helium porosimetry and mercury intrusion porosimetry characterization," *Journal of Petroleum Science and Engineering*, vol. 171, pp. 1496–1513, 2018.

[7] M. Tan, M. Su, W. Liu, X. Song, and S. Wang, "Digital core construction of fractured carbonate rocks and pore-scale analysis of acoustic properties," *Journal of Petroleum Science and Engineering*, vol. 196, article 107771, 2021.

[8] R. J. Weger, G. P. Eberli, G. T. Baechle, J. L. Massaferro, and Y. F. Sun, "Quantification of pore structure and its effect on sonic velocity and permeability in carbonates," *AAPG Bulletin*, vol. 93, no. 10, pp. 1297–1317, 2009.

[9] X. Yang, J. Fan, Y. Zhang, W. Li, Y. Du, and R. Yang, "Microscopic pore structure characteristics of tight limestone reservoirs: new insights from section 1 of the Permian Maokou formation, southeastern Sichuan Basin, China," *Unconventional Resources*, vol. 2, pp. 31–40, 2022.

[10] S. Crampin, R. McGonigle, and M. Ando, "Extensive-dilatancy anisotropy beneath Mount Hood, Oregon and the effect of aspect ratio on seismic velocities through aligned cracks," *Journal of Geophysical Research: Solid Earth*, vol. 91, no. B12, pp. 12703–12710, 1986.

[11] Q. Guo, J. Ba, C. Luo, and M. Pang, "Seismic rock physics inversion with varying pore aspect ratio in tight sandstone reservoirs," *Journal of Petroleum Science and Engineering*, vol. 207, article 109131, 2021.

[12] T. Li, Z. Wang, Y. J. Gu, R. Wang, and Y. Wang, "Experimental study of fracture structure effects on acoustic logging data using a synthetic borehole model," *Journal of Petroleum Science and Engineering*, vol. 183, article 106433, 2019.

[13] K. Verwer, G. P. Eberli, and R. J. Weger, "Effect of pore structure on electrical resistivity in carbonates," *AAPG Bulletin*, vol. 95, no. 2, pp. 175–190, 2011.

[14] J. G. Berryman, "Mixture theory for rock properties," *AGU Handbook of Physical Constants*, vol. 205–228, 2013.

[15] S. Xu and M. A. Payne, "Modeling elastic properties in carbonate rocks," *The Leading Edge*, vol. 28, no. 1, pp. 66–74, 2009.

[16] B. E. Hornby, D. L. Johnson, K. W. Winkler, and R. A. Plumb, "Fracture evaluation using reflected Stoneley-wave arrivals," *Geophysics*, vol. 54, no. 10, pp. 1274–1288, 1989.

[17] T. N. Jeppson and H. J. Tobin, "San Andreas fault zone velocity structure at SAFOD at core, log, and seismic scales," *Journal of Geophysical Research: Solid Earth*, vol. 120, no. 7, pp. 4983–4997, 2015.

[18] B. Li, W. Si, H. Shen, and X. Zhang, "Building the carbonate pore-type classifier for well logging via the blended training dataset," *Acta Geophysica*, vol. 69, no. 1, pp. 77–94, 2021.

[19] X. Tang, Z. Li, C. Hei, and Y. Su, "Elastic wave scattering to characterize heterogeneities in the borehole environment," *Geophysical Journal International*, vol. 205, no. 1, pp. 594–603, 2016.

[20] T. Li, Y. J. Gu, Z. Wang et al., "Spatiotemporal variations in crustal seismic anisotropy surrounding induced earthquakes near Fox Creek, Alberta," *Geophysical Research Letters*, vol. 46, no. 10, pp. 5180–5189, 2019.

[21] T. Li, R. Wang, Z. Wang, M. Zhao, and L. Li, "Prediction of fracture density using genetic algorithm support vector machine based on acoustic logging data," *Geophysics*, vol. 83, no. 2, pp. D49–D60, 2018.

[22] A. El-Husseiny, S. Vega, and S. Nizamuddin, "The effect of pore structure complexity and saturation history on the variations of acoustic velocity as function of brine and oil saturation in carbonates," *Journal of Petroleum Science and Engineering*, vol. 179, pp. 180–191, 2019.

[23] D. Shuai, J. Wei, B. Di, S. Yuan, J. Xie, and S. Yan, "Experimental study of fracture size effect on elastic-wave velocity dispersion and anisotropy," *Geophysics*, vol. 83, no. 1, pp. C49–C59, 2018.

[24] Z. Wang, R. Wang, F. Wang, H. Qiu, and T. Li, "Experiment study of pore structure effects on velocities in synthetic carbonate rocks," *Geophysics*, vol. 80, no. 3, pp. D207–D219, 2015.

[25] O. Yousefian, R. D. White, Y. Karbalaeisadegh, H. T. Banks, and M. Muller, "The effect of pore size and density on ultrasonic attenuation in porous structures with mono-disperse random pore distribution: a two-dimensional in-silico study," *The Journal of the Acoustical Society of America*, vol. 144, no. 2, pp. 709–719, 2018.

[26] J. J. S. De Figueiredo, J. Schleicher, R. R. Stewart et al., "Shear wave anisotropy from aligned inclusions: ultrasonic frequency dependence of velocity and attenuation," *Geophysical Journal International*, vol. 193, no. 1, pp. 475–488, 2013.

[27] Z. Zhu, M. N. Toksz, and X. Zhan, "Seismoelectric measurements in a porous quartz-sand sample with anisotropic permeability," *Geophysical Prospecting*, vol. 64, no. 3, pp. 700–713, 2016.

[28] O. V. Mikhailov, J. Queen, and M. N. Toksöz, "Using borehole electroseismic measurements to detect and characterize fractured (permeable) zones," *Geophysics*, vol. 65, no. 4, pp. 1098–1112, 2000.

[29] J. Wang, H. Hu, and W. Guan, "Experimental measurements of seismoelectric signals in borehole models," *Geophysical Journal International*, vol. 203, no. 3, pp. 1937–1945, 2015.

[30] S. Crampin, Y. Gao, and J. Bukits, "A review of retrospective stress-forecasts of earthquakes and eruptions," *Physics of the Earth and Planetary Interiors*, vol. 245, pp. 76–87, 2015.

[31] J. Zhou, Y. Jin, and M. Chen, "Experimental investigation of hydraulic fracturing in random naturally fractured blocks," *International Journal of Rock Mechanics and Mining Sciences*, vol. 47, no. 7, pp. 1193–1199, 2010.

[32] V. G. Haach, G. Vasconcelos, and P. B. Loureno, "Influence of aggregates grading and water/cement ratio in workability and hardened properties of mortars," *Construction and Building Materials*, vol. 25, no. 6, pp. 2980–2987, 2011.

[33] M. R. Shalaby and M. A. Islam, "Fracture detection using conventional well logging in carbonate Matulla formation, Geisum oil field, southern Gulf of Suez, Egypt," *Egypt. Journal of Petroleum Exploration and Production Technology*, vol. 7, no. 4, pp. 977–989, 2017.

[34] D. Han, A. Nur, and D. Morgan, "Effects of porosity and clay content on wave velocities in sandstones," *Geophysics*, vol. 51, no. 11, pp. 2093–2107, 1986.

[35] M. Kumar and D. Han, "Pore shape effect on elastic properties of carbonate rocks," in *SEG Technical Program Expanded Abstracts 2005*, Houston, Texas, 2005.

[36] S. Garia, A. K. Pal, K. Ravi, and A. M. Nair, "Laboratory assessment on factors controlling the acoustic properties of carbonates: a case study from Bombay offshore," *Journal of Petroleum Science and Engineering*, vol. 203, article 108607, 2021.

[37] K. Moravej and A. Malcolm, "Using laboratory data to understand how pore aspect ratio influences elastic parameters and amplitude variation with offset," *Geophysics*, vol. 87, no. 2, pp. T147–T156, 2022.

[38] S. Shao and L. J. Pyrak-Nolte, "Wave propagation in isotropic media with two orthogonal fracture sets," *Rock Mechanics and Rock Engineering*, vol. 49, no. 10, pp. 4033–4048, 2016.

[39] G. M. Mavko and A. Nur, "The effect of nonelliptical cracks on the compressibility of rocks," *Journal of Geophysical Research: Solid Earth*, vol. 83, no. B9, pp. 4459–4468, 1978.

[40] Z. Wang, R. Wang, R. J. Weger, T. Li, and F. Wang, "Pore-scale modeling of elastic wave propagation in carbonate rocks," *Geophysics*, vol. 80, no. 1, pp. D51–D63, 2015.

[41] L. Zhao, C. Cao, Q. Yao et al., "Gassmann consistency for different inclusion-based effective medium theories: implications for elastic interactions and poroelasticity," *Earth*, vol. 125, no. 3, p. e2019JB018328, 2020.

[42] J. G. Berryman, "Single-scattering approximations for coefficients in Biots equations of poroelasticity," *The Journal of the Acoustical Society of America*, vol. 91, no. 2, pp. 551–571, 1992.

[43] Z. Wang, G. Njiekak, D. R. Schmitt, and R.-H. Wang, "Empirical rock physics relationships on carbonate dry-frame elastic properties," *Petrol Sci*, vol. 18, pp. 783–806, 2021.

[44] Y. Chen, Y. J. Gu, L. M. Heaman, L. Wu, E. Saygin, and S. H. Hung, "Reconciling seismic structures and Late Cretaceous kimberlite magmatism in northern Alberta, Canada," *Geology*, vol. 48, no. 9, pp. 872–876, 2020.

[45] J. Nakajima, T. Matsuzawa, A. Hasegawa, and D. Zhao, "Three-dimensional structure ofVp,Vs, andVp/Vsbeneath northeastern Japan: implications for arc magmatism and fluids," *Journal of Geophysical Research: Solid Earth*, vol. 106, no. B10, pp. 21843–21857, 2001.

[46] Y. Takei, "Effect of pore geometry onVP/VS: from equilibrium geometry to crack," *Earth*, vol. 107, no. B2, p. ECV-6, 2002.

[47] M. Azadpour, A. Javaherian, M. R. Saberi, M. Shabani, and H. Shojaei, "Rock physics model-based investigation on the relationship between static and dynamic Biot's coefficients in carbonate rocks," *Journal of Petroleum Science and Engineering*, vol. 211, article 110243, 2022.

[48] X. Wang and J. J. Sheng, "Multi-scaled pore network modeling of gas-water flow in shale formations," *Journal of Petroleum Science and Engineering*, vol. 177, pp. 899–908, 2019.